OPINION

Computational morphodynamics of plants: integrating development over space and time

Adrienne H. K. Roeder, Paul T. Tarr, Cory Tobin, Xiaolan Zhang, Vijay Chickarmane, Alexandre Cunha and Elliot M. Meyerowitz

Abstract | The emerging field of computational morphodynamics aims to understand the changes that occur in space and time during development by combining three technical strategies: live imaging to observe development as it happens; image processing and analysis to extract quantitative information; and computational modelling to express and test time-dependent hypotheses. The strength of the field comes from the iterative and combined use of these techniques, which has provided important insights into plant development.

One challenge faced increasingly by developmental biologists is to understand dynamic biological processes at high spatial and temporal resolution. Time is particularly difficult to resolve because most traditional techniques achieve high spatial resolution by sample fixation, thereby preventing continuous observation of the process of interest. Live imaging, which we define as time-lapse microscopic imaging of the same living biological sample over a defined period of time, circumvents this problem[1]. Live imaging has recently advanced[2,3]. Today, fully three-dimensional (3D) live imaging at cellular resolution is achieved by observing tissues that contain fluorescent proteins and stains while imaging the organism every few hours using a confocal microscope[4] (Supplementary information S1 (figure)). This method can be used to determine how cells grow and divide, to visualize patterns and changes in gene and protein expression, and to measure cellular responses to perturbations such as cell ablations and transient gene expression.

The resultant large data sets require sophisticated analysis. Computational image processing (BOX 1) can automatically detect features of interest in the images while tracking quantitative data about those features over time.

Through live imaging, image processing and experimentation, biologists develop theoretical models. Computational models formalize these hypotheses by expressing them as a set of equations or rules that can be simulated using a computer[5–7] (TABLE 1). Computer simulations allow a quantitative comparison of the model to the data. These simulations also allow visualization of non-intuitive outcomes of complex interactions and feedback loops. Thus, computational models allow the narrowing down of a diverse set of hypotheses to a few plausible ones that can be tested experimentally.

Computational morphodynamics refers to the combined use of live imaging, image processing and computational modelling to understand morphogenesis[5]. In our opinion,

Box 1 | **Image processing**

Post-acquisition image processing and analysis provide cell measurements that can assist in the formulation and validation of computational models. Two important requirements for computing the shape, size, connectivity and position of cells from microscopy images are the generation of high quality images and the development of robust feature extraction algorithms. Noise, contrast and spatial and temporal resolution are some image quality attributes that largely control the development of image-processing algorithms and the effectiveness of their results. Acquired optical images are typically contaminated with shot noise (see the figure, part **a**); this is especially accentuated in live imaging, in which reduced light intensities are applied to avoid damaging live tissues and cells. Low image contrast, which mainly occurs in deeper parts of the tissue, hinders the separation of regions of interest from the image background. Poor spatial resolution (few slices per three-dimensional image) and temporal resolution (few images over time) are detrimental to accurately resolving the true geometry and lineage of cells during development using cell-tracking software. Reducing these image aberrations leads to enhanced image quality for visualization and promotes improvements in the delineation of regions of interest (segmentation) (see the figure, parts **b**,**c**).

Automatic image segmentation is a fundamental problem in image processing. Unfortunately, most methods usually produce only partially good results, with missing regions and edges that are sometimes difficult to automatically detect and correct. One effective approach is the semi-automatic segmentation path[62], in which faulty results are eliminated by human computation[55] (that is, by manual editing that can be done by crowds of paid workers and volunteers on the Internet) (see the figure, part **d**). In the future, interactive computer systems may be developed in which users can intervene in the segmentation process to easily and quickly repair mistakes produced by automatic programs. With the right set of interactive tools, it should be possible to mass-distribute data for corrections and scale up semi-automatic solutions to large data sets.

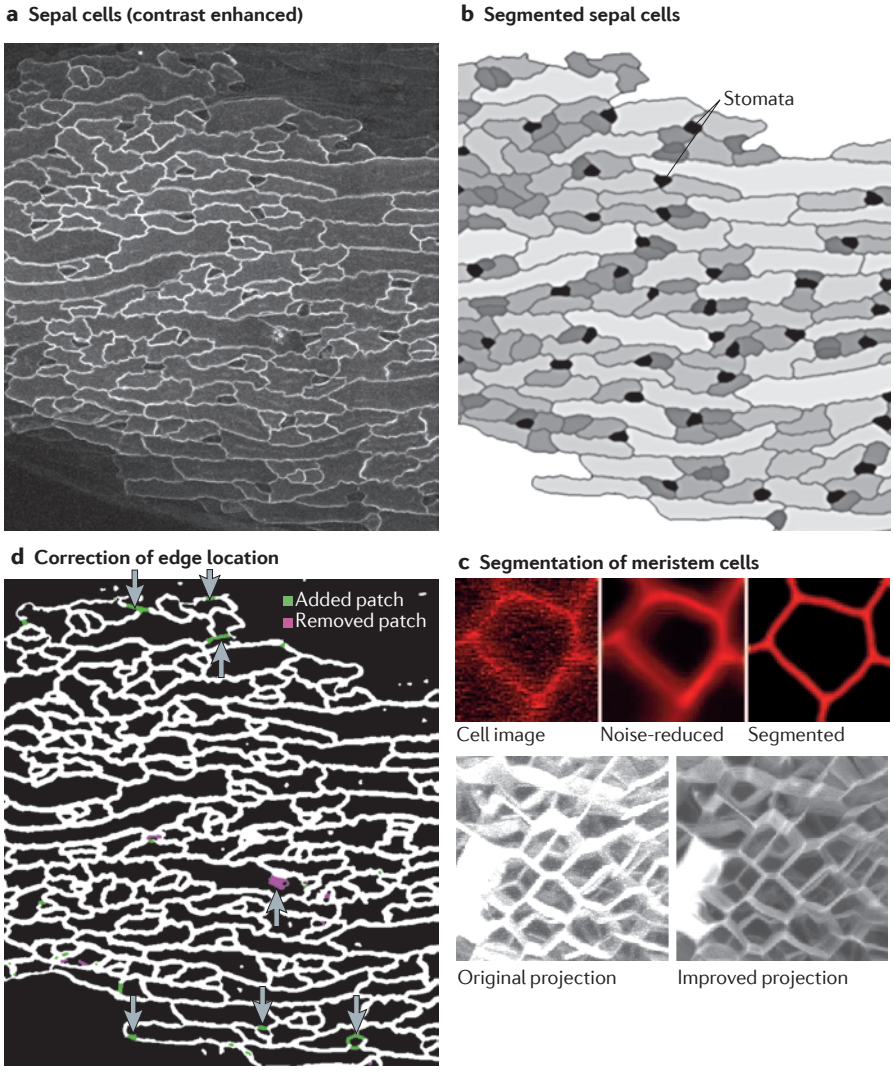

the strength of this emerging field comes from the iterative and combined use of these techniques to understand how the dynamics of molecular signalling, cellular geometry and mechanics dictate development. The field of computational morphodynamics has emerged from work with many model organisms. Such studies have provided insights into many systems, for example *Dictyostelium discoideum* morphogenesis[8], planar cell polarity in *Drosophila melanogaster*[9,10], assembly of the contractile ring for cytokinesis in yeast[11], growth of pollen tubes[12] and the patterning of leaf vasculature[13,14], among many others. In this Opinion article, we focus on the work done in plants, and specifically on what has been learned, through the integration of live imaging with computational modelling to better understand the role of molecular signalling, about cellular geometry and mechanics in the multicellular morphogenesis of plant meristems and lateral organs.

Regulatory networks in space and time

First, we examine the conclusions reached by applying computational modelling and imaging to three molecular signalling networks underlying plant morphogenesis. These examples illustrate the different levels at which modelling and imaging can be combined: cell, tissue and whole plant.

Root hair patterning. The *Arabidopsis thaliana* root epidermis is patterned into alternating files of specialized hair cells (trichoblasts) and non-hair cells (atrichoblasts). This specification is controlled both genetically and spatially (FIG. 1a). The TRANSPARENT TESTA GLABRA 1 (TTG1)–GLABRA 3 or ENHANCER OF GLABRA 3 (GL3/EGL3) transcription factor complex interacts either with the transcription factor WEREWOLF (WER), to form an active transcriptional complex specifying atrichoblast fate, or with CAPRICE (CPC), to repress *WER* expression and promote trichoblast fate. Imaging studies have shown that both CPC and GL3/EGL3 move from their sites of synthesis into the adjacent cell. *CPC* is expressed by atrichoblasts and moves into trichoblasts, where it represses *WER*. By contrast, GL3/EGL3 is expressed by trichoblasts and accumulates in the nucleus of atrichoblasts, where the transcription of the gene encoding it is otherwise repressed by WER. These imaging studies provided the basis for the initial model to explain how GL3/EGL3 is still present in atrichoblasts, despite its transcription being repressed by WER.

Table 1 | **Modelling methodologies**

Method	Description	Pros	Cons	Refs
Boolean*	Individual genes are described as ON or OFF; truth tables and state-transition graphs describe gene regulatory rules	Describes network dynamics with limited information	Detailed dynamics of gene regulatory functions cannot be determined	5,18
Differential equations*	Gene regulation is described by biophysically motivated rate laws, often represented by Michaelis–Menten-type functions	Several analytical techniques are available for probing non-linear network dynamics and for optimizing parameters	Some parameters may have to be guessed	5
Stochastic*	Simulations use probabilities based on reaction rates to decide which chemical transitions occur	Can uncover new principles on the role of noise that are due to inherent stochasticity of gene regulation and signalling	For large networks, simulations can be computationally intensive	5
Spring models‡	• Cell walls are described by springs, which connect to other cells at vertices • Equilibrium is obtained by minimizing the total elastic energy	Work well with cell division and growth	Lack resolution of finer cell wall details	5,44
Finite element methods‡	The tissue is broken up into distinct elements using various geometries, which then implement the rules of elasticity theory	Provide a detailed description of the elastic properties of cells	Are computationally intensive and cannot easily be modified for growing and dividing cells	12,57, 58
Cellular Potts methods‡	• Cells are described as a collection of similar spins, which interact with each other and the spins of neighbouring cells • A Monte Carlo scheme is employed to minimize the energy of the system and arrive at the equilibrium configuration	Used successfully in many biological cases	Dealing with motion of one cell relative to another can be problematic	43
Subcellular element method‡	Coarse-grained description of cells in terms of interacting particles that move by sensing forces from the neighbouring particles	Excellent spatial resolution	Can be computationally intensive for multicellular systems	66,67

*Models that describe cell circuit dynamics; that is, the rates of change of interacting gene and signalling network components. ‡Models that describe mechanical forces between tissues; that is, the forces within and between cells that ultimately are responsible for shaping the organ.

In addition to this genetic network, trichoblast and atrichoblast fate is determined by the position of an epidermal cell in relation to the underlying cortical layer. Epidermal cells positioned over the junction of two cortical cells become trichoblasts, whereas those directly above a cortical cell develop into atrichoblasts[15]. Genetic evidence indicates that the transmembrane receptor protein kinase SCRAMBLED (SCM; also known as SUB), which is expressed by epidermal cells, senses a signal derived from the cortical layer to repress *WER* in the epidermis[16]. It was postulated that the combined repression of *WER* by SCM and CPC results in the specification of trichoblasts, whereas the functional TTG1–GL3/EGL3–WER complex in the adjacent cell specifies atrichoblasts.

On the basis of the observations mentioned above, two computational models have been developed to elucidate this complex interaction between spatial position and the underlying genetic network. Benítez *et al.*[17] developed a model based on the assumption that *WER* self-activates. In their model stimulations, striped patterns of trichoblasts and atrichoblasts were obtained only when the SCM signal activated TTG1–GL3/EGL3–WER. However, there was no evidence to support the idea of local *WER* self-activation. This self-activation model was recently challenged by a model developed by Savage *et al.*[18], who proposed two different models that centred on the mode of regulation of *WER*. The first assumed local *WER* self-activation, with CPC repressing *WER* indirectly (the 'local *WER* self-activation' model, which is similar to that of Benítez *et al.*), whereas the second model did not include *WER* self-activation but assumed uniform *WER* transcription that was repressed by both CPC and SCM activity (the 'mutual support' model). In model simulations run in a *cpc* mutant background, the mutual support model closely matched the experimental observation of increased *WER* expression in *cpc* trichoblasts[19]. Local WER self-activation was ruled out experimentally by determining that *WER* expression is unchanged in wild-type or *wer* backgrounds. The mutual support model also correctly predicted normal *WER* expression patterns in plants mutated for both *gl3* and *egl3*. These data provide direct experimental support for the mutual support model, ruling out *WER* self-activation as a mechanism for epidermal patterning in the root.

Shoot apical meristem maintenance. At the tissue level, the use of live imaging and computational modelling have recently provided some new insights into the mechanisms that regulate the balance between stem cell renewal and differentiation at the shoot apical meristem (SAM), a structure that gives rise to the aboveground structures of flowering plants[20]. Stem cell maintenance in the SAM is regulated by the CLAVATA 1 (CLV1) receptor kinase, its ligand CLV3 and the transcription factor WUSCHEL (WUS) (FIG. 1b). The genes are expressed in a defined spatial pattern within the SAM: *CLV3* is solely expressed in the central zone, a group of pluripotent stem cells in the centre of the SAM, whereas *CLV1* and *WUS* are expressed directly below the central zone, in the rib meristem. Activation of CLV1 signalling in the rib meristem by CLV3 results in the repression of *WUS*, which is required for the production of a non-cell-autonomous signal from the rib meristem to maintain the pluripotent *CLV3*-expressing stem cells in the central zone. This feedback loop is the basis for the current model to explain the balance between stem cell renewal and differentiation. Several computational models have

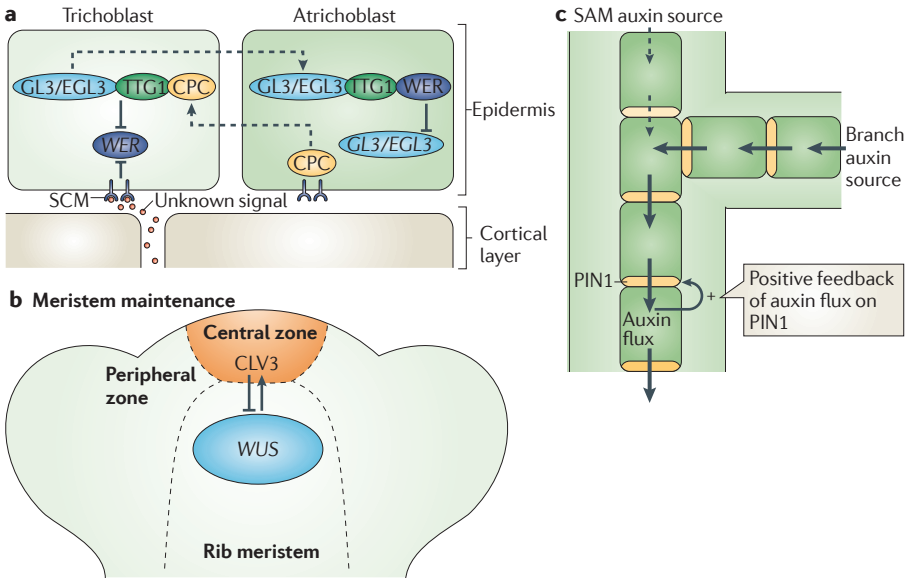

Figure 1 | **Gene regulatory networks. a** | The patterning of specialized hair cells (trichoblasts) and non-hair cells (atrichoblasts) in the root involves both spatial signalling, through the SCRAMBLED (SCM; also known as SUB) receptor, and activation or repression of transcriptional complexes that are influenced by the movement of proteins from one cell to another. Trichoblast development is initiated by the repression of *WEREWOLF* (*WER*). This is mediated by SCM, which is activated by an unknown signal secreted by cortical cells, and by CAPRICE (CPC), which moves from the atrichoblast to the trichoblast to form a transcriptional complex with TRANSPARENT TESTA GLABRA 1 (TTG1) and GLABRA 3 or ENHANCER OF GLABRA 3 (GL3/EGL3). **b** | The shoot apical meristem (SAM) can be divided into the central zone, the peripheral zone and the rib meristem[63,64]. The central zone comprises a pool of pluripotent stem cells. The peripheral zone is seated on the flanks of the SAM, where new lateral organs are initiated. *WUSCHEL* (*WUS*) is expressed exclusively in the organizing centre (blue) in the rib meristem and is required to produce an unknown signal to specify stem cell identity in the overlying cell layers. Stem cells in the central zone (orange) secrete CLAVATA 3 (CLV3), which activates a signalling cascade that limits *WUS* transcription in the rib meristem[65]. Thus, the negative feedback regulatory circuitry composed of WUS and CLV3 forms a self-correcting mechanism to maintain stem cell homeostasis in the SAM. **c** | The branching pattern of plants can be understood by modelling the competition between auxin sources at the tip of each branch to transport auxin through regions of the plant stem (represented as large boxes). A computational model in which the flux of auxin positively feeds back on the amount of the auxin efflux carrier PIN-FORMED 1 (PIN1; yellow) automatically establishes the competition between branches and reproduces the branching pattern of both wild-type and mutant plants[31].

explored how the expression patterns of *WUS* and *CLV3* are localized and interact within a static 2D longitudinal section of the meristem[21–23]. Although these models achieve spatial resolution (that is, they predict where the genes are expressed), they do not address the dynamics of growth.

Traditional molecular genetics has been successful in identifying the key components of the signalling circuit that regulates stem cell numbers in the SAM, but does not address temporal aspects of development[4]. Terminal mutant phenotypes often result from the accumulation of defects over time. For example, why is the SAM enlarged in *CLV3* loss-of-function mutants? Enlargement could be due to faster cell divisions, slower exit of cells from the central zone or increases in the WUS-mediated central zone-inducing signal. Surprisingly, live imaging together with transient inactivation of *CLV3* by RNA interference showed that none of these possibilities is correct. Instead, central zone expansion was caused by an immediate respecification of neighbouring peripheral zone cells on the boundary of central zone cells[24]. This observation could not have been made through static imaging of traditional genetic mutants, suggesting that live imaging of transient perturbations is an important strategy to visualize simultaneous changes in cell division and gene expression patterns. Geier *et al.*[25] included these insights in a population model describing the interactions between these different cell types, in which they allowed cells to both proliferate and switch fate. Simulations of this population model could accurately maintain the stable numbers of cells in each region that are observed in the SAM during proliferation. One of the challenges for the future is to integrate the genetic networks that regulate spatial patterning and respecification into a 3D growing template.

Branching. Plant branches are formed by the outgrowth of buds. Activation or repression of bud outgrowth integrates environmental inputs (such as light and nutrients), developmental signals (such as hormones and age) and genetic controls[26]. The plasticity of bud outgrowth has an essential role in determining plant architecture, crop yield and biomass production, all of which are important in agriculture.

To determine the timing and location of branch outgrowth in *A. thaliana*, individual plants were photographed daily to measure growth (kinematics)[27]. These data were used to build a descriptive computational model that reproduced the plant architecture[27]; however, the model did not elucidate which molecular mechanism controls the order in which branches grow out.

Decades ago, bud outgrowth was shown to be repressed by the downward transport of the plant hormone auxin from the shoot apex. However, the mechanism of auxin-mediated inhibition of bud outgrowth is complex and indirect[28,29]. For example, compared with wild-type plants, mutants exhibiting increased branch outgrowth can have lower levels of auxin (*transport inhibitor response 3* (*tir3*) mutants), the same levels (*auxin-resistant 1* (*axr1*) mutants) or higher levels (*more axillary branching 4* (*max4*) mutants)[30]. Without computational modelling, it is hard to give a plausible explanation for such contradictory observations. Prusinkiewicz *et al.*[31] have developed a computational model that can simulate the branching pattern of wild-type *A. thaliana* based on the assumption that there is positive feedback between the flux of auxin through a region of the plant and the concentration of the auxin efflux carrier PIN-FORMED 1 (PIN1), which transports auxin (FIG. 1c). Altering the parameters of this model is sufficient to produce increased branching similar to the mutant phenotypes observed. Thus, comparison of model simulations with branching patterns revealed by time-lapse imaging of whole plants and with mutant phenotypes led to a plausible mechanism for the complex patterns of branch outgrowth observed in nature.

Growth at the cellular level

Regulatory networks control developmental decisions, but it is the growth and division of cells that actually leads to morphogenesis. Next, we illustrate how the use of computational morphodynamics has shown that the growth and division patterns of plant cells determine the morphology of a whole tissue.

Morphogenesis of the snapdragon petal. Analysis of the growth and cell division of plants has traditionally relied on measuring the mitotic index and analysing the size and shape of clonal sectors (patches of marked sibling cells derived from a single progenitor cell)[32–34]. To generate a clonal sector, a random cell is marked visibly through an induced genetic change early in the development of the organ — for example, through the excision of a transposon near a gene controlling red pigmentation. The rate and direction of growth is inferred from the size and shape of the patch of progeny cells determined in the mature organ. However, sector analysis does not reveal which random cell was marked, when the progeny cells divided or how they gave rise to the final patch.

In the absence of live imaging, sector analysis together with imaging of the 3D shape of organs using optical projection tomography formed the biological basis for a computational model describing how simple petal primordia grow to form the complex 3D shapes of the mouth of the snapdragon (*Antirrhinum majus*) flower[35]. In this model, the tissue was treated as a continuous sheet of material that can grow in 3D. A quantitative analysis of the *in vivo* shape of wild-type and mutant petals revealed the contributions of the dorsoventral polarity genes to the growth of each region of the petal[36]. These data formed the basis for the hypothesis that dorsoventral genes control local growth rates.

However, a computational model based on this initial hypothesis was unable to replicate the exact shape of the flower or the pattern of sectors generated in the real petals. When the model was revised such that the dorsoventral genes controlled both local growth rates and the activity of hypothetical organizers of tissue polarity, it could reproduce the snapdragon mouth of both wild-type and dorsoventral-mutant flowers, as assessed by comparing the result with actual petal shapes and sectors[35,36]. Therefore, this model demonstrates a plausible mechanism of morphogenesis in snapdragon petals and enhances our understanding of how 3D shapes are generated during morphogenesis; however, the precise cellular basis of these shapes remains unknown.

Cell division and patterning in sepals. To determine the cellular basis of growth, live imaging has been used to track cell lineages and record the cell division patterns in SAMs, root meristems, floral meristems, moss buds, moss leaves and sepals (the leaf-like floral organs that envelop the developing bud)[37–41] (Supplementary information S1 (figure)). These live-imaging experiments confirm the conclusions from clonal sectors but they extend beyond this, with actual lineage traces showing the timing and orientation of all cell divisions from the progenitors onwards. One of the unique insights emerging is that the timing of cell division in many tissues is irregular[37,39,40] and that this greatly contributes to cellular patterning.

For example, a computational morphodynamics approach has indicated that irregular timing of cell division contributes to the cellular patterning in sepals[40] (FIG. 2). *A. thaliana* sepals (FIG. 2a) are characterized by the presence of highly elongated giant cells stretching about one-fifth of the length of the sepal in the outer epidermis (FIG. 2b,c). The giant cells are interspersed between cells that have a range of sizes, which raises the question: how is a range of cell sizes generated when cells are constrained by being tightly bound together by their cell walls?

Cells can become enlarged through endoreduplication, a process in which the cells replicate their DNA but fail to divide. More than a decade ago, it was proposed that diverse cell sizes would be produced if cells enter endoreduplication at different times[42]. This hypothesis was impossible to test without live imaging. Recently, tracing the cell lineages in the developing sepal epidermis confirmed that large cells enter endoreduplication early and small cells enter endoreduplication later[40] (FIG. 2f). Based on these observations, a growing sepal was computationally modelled as an expanding template of cells, each of which could divide or enter endoreduplication with certain probabilities (FIG. 2g) that were estimated from the data (FIG. 2d,e). However, a simple model of this hypothesis was unable to match the actual *in vivo* cell size distribution (as measured using image processing (BOX 1)).

A modified hypothesis arose from a detailed examination of cell divisions by live imaging, which revealed that the length of the cell cycle is highly variable and also correlates with cell size. A computational model in which cells have both a certain probability of endoreduplicating and a random cell cycle length reproduced the observed cell areas, suggesting that variability in cell division is a plausible mechanism for generating cell size diversity (FIG. 2g–j). Furthermore, by changing the probability of endoreduplication in the first cell cycle, the model could predict the cell size distribution for loss-of-function mutants with too few giant cells and gain-of-function mutants with too many giant cells, thereby validating the model (FIG. 2i,j). The conclusion that the stochasticity in the timing of cell division and in the decision to endoreduplicate together produce a range of cell sizes within a growing organ could be reached only by combining live imaging, modelling and image processing[40].

Mechanics influences organ initiation

The previous examples have discussed how gene regulatory networks and growth contribute to patterning and morphogenesis; however, these processes take place in a physical framework in which mechanical forces between cells can influence the final form of the tissue. Below, we show that a computational morphodynamics approach has shaped our understanding of how mechanical signalling affects organ initiation.

Phyllotaxis and rhizotaxis by polarized auxin transport. In shoot and root tissue, local maxima (peak concentrations) in the concentration of the plant hormone auxin specify the location of organ outgrowth. Modelling has shown that these local maxima can be generated by polarized auxin transport mediated by PIN proteins[43–45].

In the root, lateral root primordia are initiated from the twin files of pericycle cells (specialized cells that are located outside the vascular tissues) at irregular intervals. Lateral root formation commonly correlates with higher-than-average levels of auxin perception, especially at the outer convex side of the root[46,47]. Reduction in auxin perception or transport in the root decreases the density of lateral roots, and activation of auxin synthesis in pericycle cells initiates the formation of lateral root primordia[48–50].

Similarly, early biochemical and genetic experiments showed that transport of auxin is necessary for the specification of organs in the SAM[51]. Experiments with the tomato SAM further confirmed that local auxin accumulation was both necessary and sufficient for the induction of organ growth around the SAM[52]. However, by the end of the twentieth century, it was still not known how auxin acted in the SAM to form organs. Subsequent live-imaging experiments showed that the polarization of PIN1 in the SAM epidermis resulted in local auxin

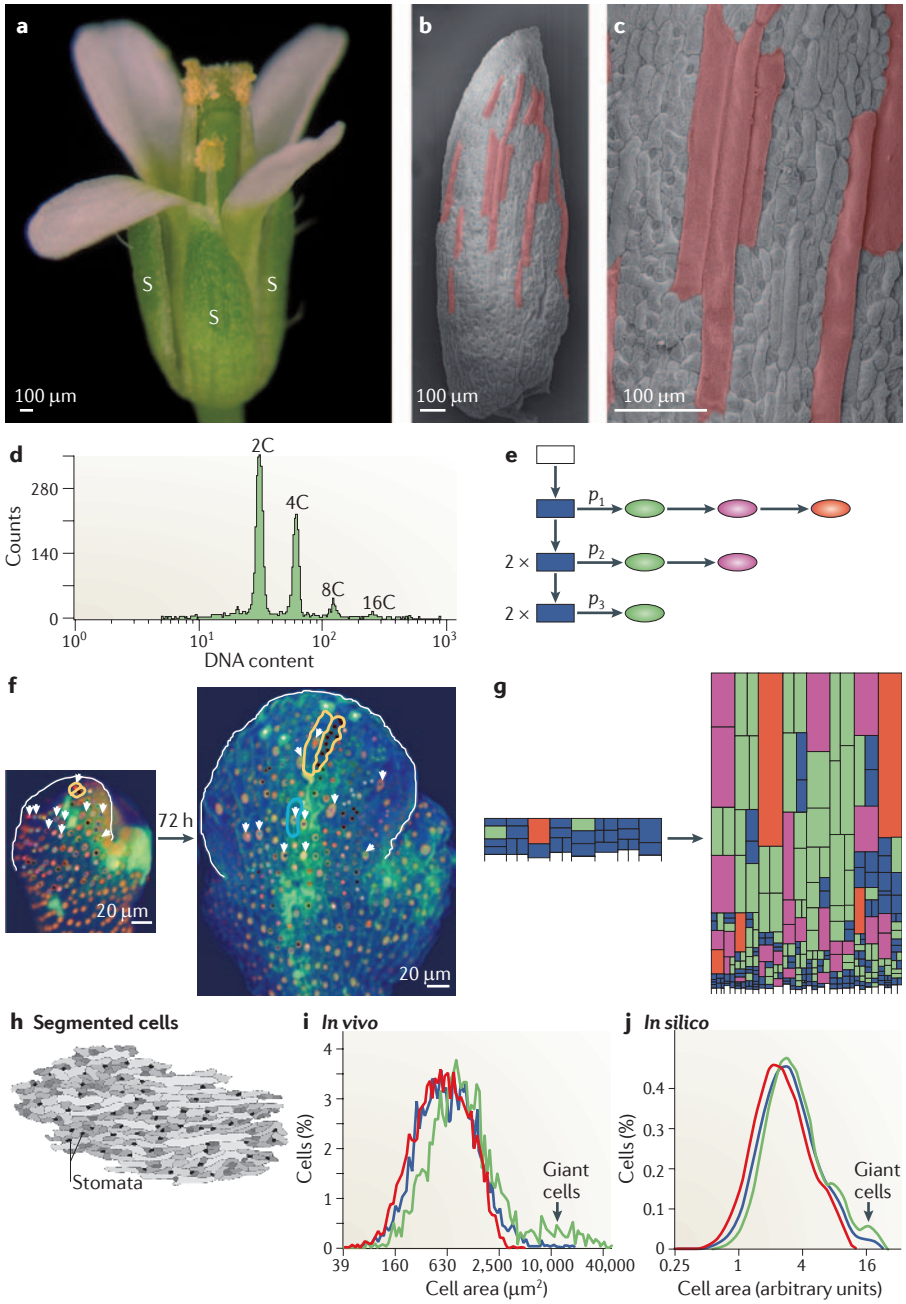

Figure 2 | **The iterative process of imaging, image processing and modelling in sepal patterning.** **a**–**c** | The sepals (S) of a wild-type flower can be of diverse cell sizes, ranging from giant cells (false-coloured pink) to small cells (uncoloured grey). **d**,**e** | The ploidy (number of chromosomes (C)) of cells was measured using flow cytometry to determine how many rounds of endoreduplication (a cell cycle that includes DNA replication but not division) sepal cells had undergone (**d**). The ploidy data formed the basis for a population model (**e**), in which cells can divide (arrow down) or endoreduplicate (arrow right). The model was used to predict the probability (*p*) with which each cell will enter endoreduplication at each time (subscript on *p*). The colour represents the ploidy of the cell: blue = 2C; green = 4C; magenta = 8C; and red = 16C. **f**,**g** | Live imaging shows the growth of a sepal over 72 hours and the lineages of the cells (marked with the same coloured dots). Analysis of the live-imaging sequence revealed that both the timing of endoreduplication and the timing of cell division are highly variable (**f**). A geometric growth model (**g**) of sepal giant cell development based on this timing data from live imaging (**f**) and probability of endoreduplication as determined by the population model (**e**) predicts the diversity of cell areas. The colour represents the ploidy of the cell, as above. **h**–**j** | A crucial step in validating the model was using image processing (**h** and BOX 1) to obtain the distribution of cell areas *in vivo* (**i**), which was compared with the model predictions (**j**). The model agreed well with measured areas for wild type (blue). In addition, perturbations of the model matched genetically altered plants with too few (red) or too many (green) giant cells. Images in parts **a**–**g**, **i** and **j** are modified from REF. 40.

maxima where organs would later arise[53–56]. These live-imaging data were used to construct two separate computational models of auxin-based patterning in the shoot. In both models, the observed auxin maxima were generated when PIN1 was polarized towards the neighbouring cell that had the highest concentration of auxin. However, these models were based on hypothetical mechanisms whereby cells needed to sense the concentration of auxin in their neighbours[44,45]. The mechanism by which this polarization could occur remained a mystery until more recent examination of tissue mechanics using computational morphodynamics (see below).

Mechanics orients cell polarity. Biologists have long understood that the final form of a tissue is connected with specific genetic programmes. But how the mechanical properties of those tissues affect their final form was hard to study owing to inherent technical limitations, such as measuring cellular stress within a tissue. In plants, this is particularly relevant because cells adhere to their neighbours; therefore, any local mechanical change is propagated throughout the tissue. Recently, live imaging and computational modelling were used to test the hypothesis that the mechanical properties of the SAM epidermis determine the positions of new organs[57,58]. It has long been observed that the orientation of cell wall microfibrils aligns with the orientation of microtubules, as microtubules serve as tracks for the enzymes involved in cellulose synthesis. Using a live-imaging data set, a realistic SAM template was extracted from a confocal image stack for modelling simulations. Computational analysis of stress patterns revealed that the direction of stress of each cell accurately predicted the microtubule orientations observed by live imaging[57] (FIG. 3a). Furthermore, the model could predict the circumferential reorientation of microtubules around a wound site following cell ablation (a mechanical perturbation), as observed by live imaging (FIG. 3b). Likewise, live imaging showed that PIN1 polarized towards anticlinal cell walls parallel to the microtubule arrays, which suggested that stress patterns have a role in PIN polarization and therefore in the direction of auxin transport[58] (FIG. 3a,b). Simulations of an updated model, in which PIN1 localizes towards the most stressed walls, were able to produce a phyllotactic pattern. Thus, live imaging and modelling were instrumental in reaching the conclusion that, in plants, mechanics is a plausible mechanism for

coordinating the extent of growth (mediated by auxin) with the direction of growth (mediated by microtubules).

The observation that lateral root primordia are initiated on the outer surfaces of bends in the root suggests a role for mechanical stresses in lateral root initiation as well. A recent study coupled live imaging with computational modelling and showed that alterations in cell length at the sites of curvature can induce auxin maxima that are required for lateral root initiation[59]. Imaging of the expression levels and patterns of PIN proteins in the different developmental zones of the root was used to produce parameters for a model of root auxin flux. This showed that the organization of PIN proteins in the root leads to the formation of local auxin reflux loops that are further reinforced by the flux of auxin through the root tissue at sites of curvature. Live imaging of auxin transporter 1 (AUX1; which imports auxin into cells) showed that the AUX1–yellow fluorescent protein signal intensified on the membranes of the pericycle cell at the apex of curvature (FIG. 3c). Updating the model to include a positive feedback loop for AUX1 in auxin accumulation indicated that auxin peaks become localized to a few outer pericycle cells that correspond to where *in silico* roots are curved in model simulations (FIG. 3d). These studies reveal that mechanics is involved in producing local auxin maxima and therefore in generating developmental patterns in both the root and the shoot.

Perspectives

The question of how cellular signals interact with tissue mechanics has been difficult to address with traditional methods; therefore, morphogenesis is poorly understood. Computational morphodynamics is a way forward in integrating aspects of physics, chemistry and computer science with biology to understand how genes regulate the behaviour of cells, how cells interact to give rise to tissues and how tissues are structured into organs in the final form of an organism.

Although the computational morphodynamics approach is still in its infancy, its use in both plants and animals is expanding[6]. Many studies have used either live imaging or computational modelling[5–7] effectively, and the integration of these approaches has led to conclusions that could not have been reached otherwise. Computational modelling is helpful for examining systems with many variables or parameters that are difficult to directly measure. Live imaging reveals dynamic processes that cannot be fully understood by looking at fixed samples. In addition, image processing is required to quantitatively understand the collected data in a robust and repeatable way. In this Opinion article, we have highlighted the insights gained from a few studies in plants in which imaging, image processing and computational modelling were combined.

The limitations of the computational morphodynamics approach are technical (in imaging, image processing, model development and processing power), but these limitations are being addressed by the development of new technologies and techniques. For example, new fluorescent sensors, probes and markers allow imaging of new systems, such as small molecules, hormone gradients and protein–protein interactions. New microscopes may allow access to cells deeper in tissues and the generation of higher-resolution images. New image-processing strategies allow automatic or semi-automatic identification and tracking of cells, such that greater quantities of increasingly complex data can be used[41,60,61]. New modelling methodologies may allow the development of more accurate models of the properties of growing and dividing

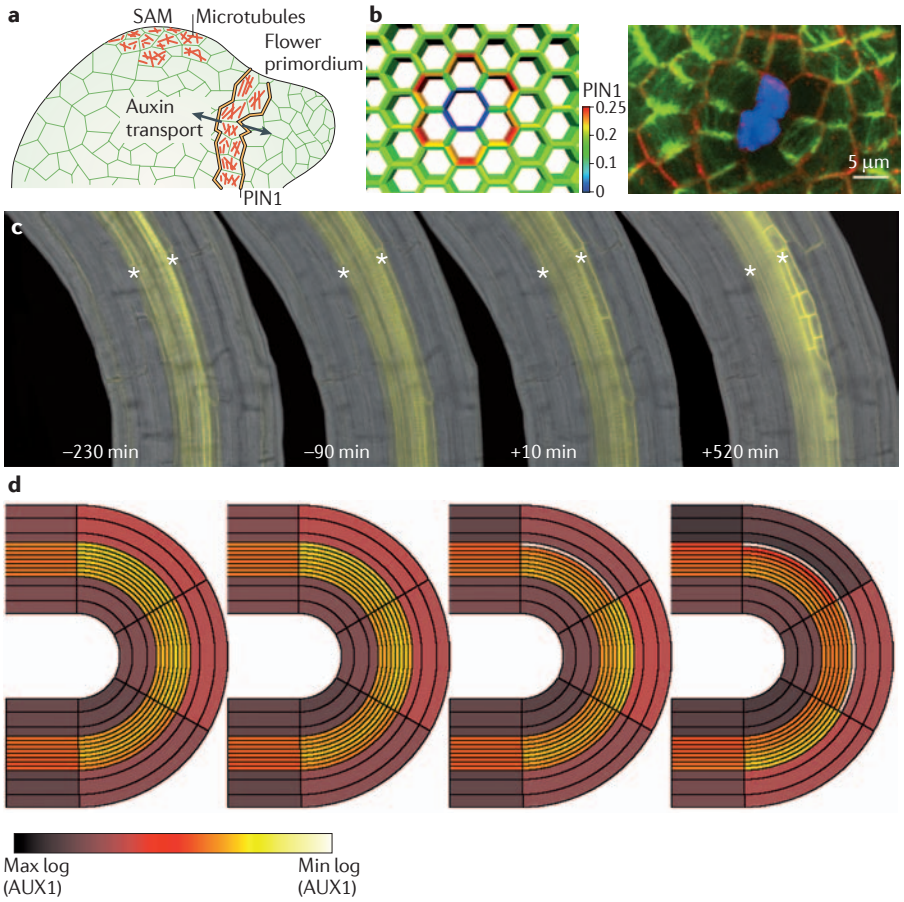

Figure 3 | **Mechanics. a** | At the boundaries between the shoot apical meristem (SAM) and the flower primordia, the anisotropic mechanical stress of the cells orients the microtubules (red) around the primordia. The stress also polarizes PIN-FORMED 1 (PIN1; yellow), such that auxin is transported both towards the new organ and towards the next site of organ formation (indicated by arrows). By contrast, in the centre of the meristem, patterns of both PIN1 and microtubules are more irregular, reflecting stress patterns that are equally distributed between cells at the shoot apex (isotropy). **b** | A model (left) of the change in the mechanical stress pattern after the ablation of a cell (blue) predicts that PIN1 (red) will relocalize to point away from the ablated cell. Live imaging (right) shows that, in agreement with the model, both PIN1 (red) and microtubules (green) reorient to point away from the ablation site (blue). **c** | Live imaging of the accumulation of auxin transporter 1 (AUX1; yellow) accumulation in the outer pericycle cell layer (indicated by asterisks) at sites of curvature before and after the first cell division (time 0 min), marking the formation of a lateral root primordium. **d** | Modelling results based on live imaging show that cell elongation can cause an increase in auxin concentration (not shown) and AUX1 expression when the positive feedback of AUX1 is added to the model parameters. Images in part **b** are reproduced from REF. 58. Images in parts **c** and **d** are reproduced from REF. 59.

cells. Although technology will no doubt provide us with better tools, we must understand that technology alone will not deliver a complete and holistic understanding of development. Arriving at the ultimate goal of constructing 'computable' plants and animals will also require cogent experiments and creative hypotheses to be explored using computational morphodynamics.

Adrienne H. K. Roeder, Paul T. Tarr, Cory Tobin, Xiaolan Zhang, Vijay Chickarmane and Elliot M. Meyerowitz are at the Division of Biology 156-29, California Institute of Technology, 1200 E. California Blvd, Pasadena, California 91125, USA.

Alexandre Cunha is at the Center for Advanced Computing Research MC 158-79, California Institute of Technology, 1200 E. California Blvd, Pasadena, California 91125, USA.

Correspondence to A.H.K.R. and E.M.M.
e-mails: aroeder@caltech.edu; meyerow@caltech.edu

doi:10.1038/nrm3079
Published online 2 March 2011

1. Reddy, G. V. & Roy-Chowdhury, A. Live-imaging and image processing of shoot apical meristems of *Arabidopsis thaliana*. *Methods Mol. Biol.* **553**, 305–316 (2009).
2. Ball, E. Cell division patterns in living shoot apices. *Phytomorphology* **10**, 377–396 (1960).
3. Dumais, J. & Kwiatkowska, D. Analysis of surface growth in shoot apices. *Plant J.* **31**, 229–241 (2002).
4. Reddy, G. V., Gordon, S. P. & Meyerowitz, E. M. Unravelling developmental dynamics: transient intervention and live imaging in plants. *Nature Rev. Mol. Cell Biol.* **8**, 491–501 (2007).
5. Chickarmane, V. *et al.* Computational morphodynamics: a modeling framework to understand plant growth. *Annu. Rev. Plant Biol.* **61**, 65–87 (2010).
6. Oates, A. C., Gorfinkiel, N., González-Gaitán, M. & Heisenberg, C. P. Quantitative approaches in developmental biology. *Nature Rev. Genet.* **10**, 517–530 (2009).
7. Grieneisen, V. A. & Scheres, B. Back to the future: evolution of computational models in plant morphogenesis. *Curr. Opin. Plant Biol.* **12**, 606–614 (2009).
8. Sawai, S., Thomason, P. A. & Cox, E. C. An autoregulatory circuit for long-range self-organization in *Dictyostelium* cell populations. *Nature* **433**, 323–326 (2005).
9. Aigouy, B. *et al.* Cell flow reorients the axis of planar polarity in the wing epithelium of *Drosophila*. *Cell* **142**, 773–786.
10. Amonlirdviman, K. *et al.* Mathematical modeling of planar cell polarity to understand domineering nonautonomy. *Science* **307**, 423–426 (2005).
11. Vavylonis, D., Wu, J. Q., Hao, S., O'Shaughnessy, B. & Pollard, T. D. Assembly mechanism of the contractile ring for cytokinesis by fission yeast. *Science* **319**, 97–100 (2008).
12. Fayant, P. *et al.* Finite element model of polar growth in pollen tubes. *Plant Cell* **22**, 2579–2593 (2010).
13. Scarpella, E., Marcos, D., Friml, J. & Berleth, T. Control of leaf vascular patterning by polar auxin transport. *Genes Dev.* **20**, 1015–1027 (2006).
14. Bayer, E. M. *et al.* Integration of transport-based models for phyllotaxis and midvein formation. *Genes Dev.* **23**, 373–384 (2009).
15. Galway, M. E. *et al.* The *TTG* gene is required to specify epidermal cell fate and cell patterning in the *Arabidopsis* root. *Dev. Biol.* **166**, 740–754 (1994).
16. Kwak, S. H., Shen, R. & Schiefelbein, J. Positional signaling mediated by a receptor-like kinase in *Arabidopsis*. *Science* **307**, 1111–1113 (2005).
17. Benítez, M., Espinosa-Soto, C., Padilla-Longoria, P., Díaz, J. & Alvarez-Buylla, E. R. Equivalent genetic regulatory networks in different contexts recover contrasting spatial cell patterns that resemble those in *Arabidopsis* root and leaf epidermis: a dynamic model. *Int. J. Dev. Biol.* **51**, 139–155 (2007).
18. Savage, N. S. *et al.* A mutual support mechanism through intercellular movement of CAPRICE and GLABRA3 can pattern the *Arabidopsis* root epidermis. *PLoS Biol.* **6**, e235 (2008).
19. Lee, M. M. & Schiefelbein, J. Cell pattern in the *Arabidopsis* root epidermis determined by lateral inhibition with feedback. *Plant Cell* **14**, 611–618 (2002).
20. Steeves, T. A. & Sussex, I. M. *Patterns in Plant Development* (Cambridge Univ. Press, Cambridge, UK, 1989).
21. Hohm, T., Zitzler, E. & Simon, R. A dynamic model for stem cell homeostasis and patterning in *Arabidopsis* meristems. *PLoS ONE* **5**, e9189 (2010).
22. Jönsson, H. *et al.* Modeling the organization of the WUSCHEL expression domain in the shoot apical meristem. *Bioinformatics* **21**, I232–I240 (2005).
23. Nikolaev, S. V., Penenko, A. V., Lavreha, V. V., Mjolsness, E. D. & Kolchanov, N. A. A model study of the role of proteins CLV1, CLV2, CLV3, and WUS in regulation of the structure of the shoot apical meristem. *Russ. J. Dev. Biol.* **38**, 383–388 (2007).
24. Reddy, G. V. & Meyerowitz, E. M. Stem-cell homeostasis and growth dynamics can be uncoupled in the *Arabidopsis* shoot apex. *Science* **310**, 663–667 (2005).
25. Geier, F. *et al.* A quantitative and dynamic model for plant stem cell regulation. *PLoS ONE* **3**, e3553 (2008).
26. Domagalska, M. A. & Leyser, O. Signal integration in the control of shoot branching. *Nature Rev. Mol. Cell Biol.* **12**, 211–221 (2011).
27. Mundermann, L., Erasmus, Y., Lane, B., Coen, E. & Prusinkiewicz, P. Quantitative modeling of *Arabidopsis* development. *Plant Physiol.* **139**, 960–968 (2005).
28. Hall, S. M. & Hillman, J. R. Correlative inhibition of lateral bud growth in *Phaseolus vulgaris* L. timing of bud growth following decapitation. *Planta* **123**, 137–143 (1975).
29. Thimann, K. V., Skoog, F. & Kerckhoff, W. G. On the inhibition of bud development and other functions of growth substance in *Vicia faba*. *Proc. R. Soc. Lond. B* **114**, 317–339 (1934).
30. Stirnberg, P., Ward, S. & Leyser, O. Auxin and strigolactones in shoot branching: intimately connected? *Biochem. Soc. Trans.* **38**, 717–722 (2010).
31. Prusinkiewicz, P. *et al.* Control of bud activation by an auxin transport switch. *Proc. Natl Acad. Sci. USA* **106**, 17431–17436 (2009).
32. Bossinger, G. & Smyth, D. R. Initiation patterns of flower and floral organ development in *Arabidopsis thaliana*. *Development* **122**, 1093–1102 (1996).
33. Irish, V. F. & Sussex, I. M. A fate map of the *Arabidopsis* embryonic shoot apical meristem. *Development* **115**, 745–753 (1992).
34. Poethig, R. S. & Sussex, I. M. The cellular parameters of leaf development in tobacco: a clonal analysis. *Planta* **165**, 170–184 (1985).
35. Green, A. A., Kennaway, J. R., Hanna, A. I., Bangham, J. A. & Coen, E. Genetic control of organ shape and tissue polarity. *PLoS Biol.* **8**, e1000537 (2010).
36. Cui, M. L., Copsey, L., Green, A. A., Bangham, J. A. & Coen, E. Quantitative control of organ shape by combinatorial gene activity. *PLoS Biol.* **8**, e1000538 (2010).
37. Campilho, A., Garcia, B., Toorn, H. V., Wijk, H. V. & Scheres, B. Time-lapse analysis of stem-cell divisions in the *Arabidopsis thaliana* root meristem. *Plant J.* **48**, 619–627 (2006).
38. Harrison, C. J., Roeder, A. H., Meyerowitz, E. M. & Langdale, J. A. Local cues and asymmetric cell divisions underpin body plan transitions in the moss *Physcomitrella patens*. *Curr. Biol.* **19**, 461–471 (2009).
39. Reddy, G. V., Heisler, M. G., Ehrhardt, D. W. & Meyerowitz, E. M. Real-time lineage analysis reveals oriented cell divisions associated with morphogenesis at the shoot apex of *Arabidopsis thaliana*. *Development* **131**, 4225–4237 (2004).
40. Roeder, A. H. K. *et al.* Variability in the control of cell division underlies sepal epidermal patterning in *Arabidopsis thaliana*. *PLoS Biol.* **8**, e1000367 (2010).
41. Fernandez, R. *et al.* Imaging plant growth in 4D: robust tissue reconstruction and lineaging at cell resolution. *Nature Methods* **7**, 547–553 (2010).
42. Traas, J., Hulskamp, M., Gendreau, E. & Hofte, H. Endoreduplication and development: rule without dividing? *Curr. Opin. Plant Biol.* **1**, 498–503 (1998).
43. Grieneisen, V. A., Xu, J., Maree, A. F., Hogeweg, P. & Scheres, B. Auxin transport is sufficient to generate a maximum and gradient guiding root growth. *Nature* **449**, 1008–1013 (2007).
44. Jönsson, H., Heisler, M. G., Shapiro, B. E., Meyerowitz, E. M. & Mjolsness, E. An auxin-driven polarized transport model for phyllotaxis. *Proc. Natl Acad. Sci. USA* **103**, 1633–1638 (2006).
45. Smith, R. S. *et al.* A plausible model of phyllotaxis. *Proc. Natl Acad. Sci. USA* **103**, 1301–1306 (2006).
46. Fortin, M. C., Pierce, F. J. & Poff, K. L. The pattern of secondary root formation in curving roots of *Arabidopsis thaliana* (L.) Heynh. *Plant Cell Environ.* **12**, 337–339 (1989).
47. De Smet, I. *et al.* Auxin-dependent regulation of lateral root positioning in the basal meristem of *Arabidopsis*. *Development* **134**, 681–690 (2007).
48. Boerjan, W. *et al. superroot*, a recessive mutation in *Arabidopsis*, confers auxin overproduction. *Plant Cell* **7**, 1405–1419 (1995).
49. Dubrovsky, J. G. *et al.* Auxin acts as a local morphogenetic trigger to specify lateral root founder cells. *Proc. Natl Acad. Sci. USA* **105**, 8790–8794 (2008).
50. Fukaki, H., Tameda, S., Masuda, H. & Tasaka, M. Lateral root formation is blocked by a gain-of-function mutation in the *SOLITARY-ROOT/IAA14* gene of *Arabidopsis*. *Plant J.* **29**, 153–168 (2002).
51. Okada, K., Ueda, J., Komaki, M. K., Bell, C. J. & Shimura, Y. Requirement of the auxin polar transport system in early stages of *Arabidopsis* floral bud formation. *Plant Cell* **3**, 677–684 (1991).
52. Reinhardt, D., Mandel, T. & Kuhlemeier, C. Auxin regulates the initiation and radial position of plant lateral organs. *Plant Cell* **12**, 507–518 (2000).
53. Benkova, E. *et al.* Local, efflux-dependent auxin gradients as a common module for plant organ formation. *Cell* **115**, 591–602 (2003).
54. Heisler, M. G. *et al.* Patterns of auxin transport and gene expression during primordium development revealed by live imaging of the *Arabidopsis* inflorescence meristem. *Curr. Biol.* **15**, 1899–1911 (2005).
55. Reinhardt, D. *et al.* Regulation of phyllotaxis by polar auxin transport. *Nature* **426**, 255–260 (2003).
56. Vernoux, T., Kronenberger, J., Grandjean, O., Laufs, P. & Traas, J. PIN-FORMED 1 regulates cell fate at the periphery of the shoot apical meristem. *Development* **127**, 5157–5165 (2000).
57. Hamant, O. *et al.* Developmental patterning by mechanical signals in *Arabidopsis*. *Science* **322**, 1650–1655 (2008).
58. Heisler, M. G. *et al.* Alignment between PIN1 polarity and microtubule orientation in the shoot apical meristem reveals a tight coupling between morphogenesis and auxin transport *PLoS Biol.* **8**, e1000516 (2010).
59. Laskowski, M. *et al.* Root system architecture from coupling cell shape to auxin transport. *PLoS Biol.* **6**, e307 (2008).
60. Gor, V., Elowitz, M., Bacarian, T. & Mjolsness, E. Tracking cell signals in fluorescent images in *Proc. 2005 IEEE Comp. Soc. Conf. on Computer Vision and Pattern Recognition* 142 (2005).
61. Liu, M., Roy-Chowdhury, A. K. & Reddy, G. V. Robust estimation of stem cell lineages using local graph matching in *IEEE Comp. Soc. Workshop on Mathematical Methods in Biomedical Image Analysis* 194 (2009).
62. Cunha, A., Roeder, A. & Meyerowitz, E. M. Segmenting the sepal and shoot apical meristem of *Arabidopsis thaliana* in *Eng. Med. Biol. Soc. (EMBC), 2010 Ann. Int. Conf. IEEE* 5338–5342 (2010).
63. Clark, S. E. Cell signalling at the shoot meristem. *Nature Rev. Mol. Cell Biol.* **2**, 276–284 (2001).
64. Nishimura, A., Tamaoki, M., Sato, Y. & Matsuoka, M. The expression of tobacco *knotted1*-type class 1 homeobox genes correspond to regions predicted by the cytohistological zonation model. *Plant J.* **18**, 337–347 (1999).
65. Xie, M., Tataw, M. & Venugopala Reddy, G. Towards a functional understanding of cell growth dynamics in shoot meristem stem-cell niche. *Semin. Cell Dev. Biol.* **20**, 1126–1133 (2009).

66. Sandersius, S. A. & Newman, T. J. Modeling cell rheology with the Subcellular Element Model. *Phys. Biol.* **5**, 015002 (2008).
67. Van Liedekerke, P. *et al.* A particle-based model to simulate the micromechanics of single-plant parenchyma cells and aggregates. *Phys. Biol.* **7**, 026006 (2010).

Acknowledgements
We apologize to the numerous members of these fields whose work we could not include owing to space limitations. We thank E. Mjolsness, W. Li, Y. Zhou and L. Ben-Ghaly for insightful comments. We acknowledge support from the Gordon and Betty Moore Cell Center at California Institute of Technology, the US National Institutes of Health (grants F32GM090543 to P.T.T. and R01 GM086639 to E.M.M.), the US Department of Energy (grant DE-FG02-88ER13873 to E.M.M.) and the US National Science Foundation (grant IOS-0846192 to E.M.M.).

Competing interests statement
The authors declare no competing financial interests.

FURTHER INFORMATION
Elliot M. Meyerowitz's homepage:
http://www.its.caltech.edu/~plantlab

SUPPLEMENTARY INFORMATION
See online article: S1 **(figure)**

ALL LINKS ARE ACTIVE IN THE ONLINE PDF